INTERNATIONAL JOURNAL OF AUTOMOTIVE AND MECHANICAL ENGINEERING
ISSN: 2229-8649 e-ISSN: 2180-1606
VOLUME 22, ISSUE 4, 2025, 13031 - 13042
DOI: https://doi.org/10.15282/ijame.22.4.2025.15.0992

RESEARCH ARTICLE

Tool Wear Identification and Monitoring of Hard Alloy End Mills Using an Improved WOA and ConvLSTM

Pan Yang

School of Intelligent Manufacturing, Chongqing Industry & Trade Polytechnic, 408000 Chongqing, China

ABSTRACT – The wear state of carbide end mills directly affects the processing efficiency and quality. Traditional methods (such as Support Vector Machine (SVM)) have problems such as insufficient feature extraction and poor robustness when dealing with high-dimensional nonlinear data. To this end, an SVM classification model optimized by the Whale Optimization Algorithm (WOA) is proposed. The study combines the Convolutional Long Short-Term Memory (ConvLSTM) network and the Attention Mechanism (AM) to construct the wear prediction model (ConvLSTM-AM). Experiments show that the average classification accuracy of SVM-WOA for the four types of wear exceeds 97%, and the classification time is only 1.15 seconds. The prediction accuracy of ConvLSTM-AM in the severe wear stage reaches 98.64%, and the prediction error is significantly lower than that of the comparison models. This method provides an efficient solution for real-time monitoring and intelligent maintenance of tool wear.

ARTICLE HISTORY
Received : 11th Oct. 2024
Revised : 13th May 2025
Accepted : 18th Sept. 2025
Published : 19th Nov. 2025

KEYWORDS
WOA
LSTM
ID-CNN
End mill
Wear identification
SVM

1. INTRODUCTION

1.1 Background

Hard alloy end mills stand as crucial machining tools within the manufacturing sector, with their wear state exerting a direct influence on both machining efficiency and product quality. Long-term use of end mills can easily lead to tool wear, resulting in reduced machining accuracy and even equipment failure [1-2]. Therefore, the effective identification and ongoing surveillance of the wear status of hard alloy end mills have attracted significant attention from researchers and practitioners alike. In recent years, with the continuous development of intelligent manufacturing technology, data-driven methods for wear identification and monitoring have gradually gained attention and application [3]. The current research mainly focuses on using traditional signal processing and machine learning methods for wear identification and monitoring. These methods analyze various signal characteristics and then combine them with classification algorithms to identify the wear state. However, traditional classification methods, such as Support Vector Machine (SVM), cannot fully explore the deep features in signals when processing high-dimensional and nonlinear data, which can easily lead to insufficient recognition accuracy and robustness [4].

To address these issues, deep learning methods have been gradually introduced into wearable recognition. Among them, Convolutional Neural Networks (CNN) and Long Short-Term Memory (LSTM) are widely used due to their advantages in feature extraction and time series processing. However, traditional CNN and LSTM models still face difficulties in parameter optimization and long training times when dealing with complex data [5]. Against this backdrop, the study first innovatively utilizes the Whale Optimization Algorithm (WOA) to optimize SVM, and then builds a recognition and classification model that combines WOA and SVM. Secondly, the study innovatively combines Convolutional Long Short-Term Memory Network (ConvLSTM) and Attention Mechanism (AM) to build a wear prediction model, aiming to enhance the recognition ability of traditional LSTM for wear features and achieve accurate prediction of different wear stages.

The research is divided into four sections. The first section is the introduction, which summarizes and elaborates on the background of the research question and the research motivation. The second section is the method section, which provides a detailed introduction to the wear state recognition model based on SVM-WOA and the wear state prediction model based on the improved ConvLSTM proposed in the research. The third section is the experimental section, which analyzes the classification and prediction performance of the model proposed in the research. The fourth section is the conclusion section, which introduces and summarizes the research content and achievements, and provides prospects for future research.

1.2 Related work

The process of identifying and monitoring end mill wear involves the detection and assessment of wear conditions on end mills while they are in operation, which is achieved through a variety of technical methods. In recent years, many scholars have conducted research on this topic. Huang W et al. utilized acoustic emission sensors to detect wear on electroplated diamond grinding tools. Two distinct methods were employed to analyze acoustic emission signals. The model could accurately identify the wear characteristics of different wear stages [6]. Pyatykh et al. used sound signal

*CORRESPONDING AUTHOR | Pan Yang | ✉ yangpan_199009@163.com

spectrum analysis to evaluate tool wear during the stainless-steel end milling process. This study eliminated vibration through modal analysis and analyzed the frequency spectrum of sound signals using the fast Fourier transform method. This method enabled an objective assessment of both the extent and the nature of normal tool wear. Its real-time detection outcomes could effectively prevent tool breakage, mitigate economic losses stemming from scrapped workpieces and production downtime, thereby enhancing tool efficiency [7]. Peng et al. proposed a tool wear recognition method with single sensor signals. By employing a hybrid model comprising a deep CNN and stacked LSTM, a sophisticated mapping relationship was established. The method can be effectively applied to tool wear identification under a single sensor signal. The average root mean square error (RMSE) and mean absolute error (MAE) were reduced to 9.43 and 7.15, respectively, compared with the values before optimization [8]. Wang et al. proposed a novel method for tool wear monitoring using a non-negative constraint autoencoder and an improved Grey Wolf Optimization (GWO) algorithm to address the complexity of identifying tool states during milling processes that are difficult to effectively identify. This method extracted features from multi-source heterogeneous signals and used deep networks for feature fusion. This method performed well [9].

Shah et al. constructed a method with signal wavelet analysis and an LSTM model. This method utilized a single sample generative adversarial network and trained three types of LSTM models. The stacked LSTM model performed the best in vibration signal prediction [10]. Nam et al. designed a tool for a fracture monitoring system based on acoustic emission signals and deep learning models. They constructed and trained an LSTM autoencoder with acoustic emission signals, cutting speed, spindle speed, and cutting depth as input data to distinguish between normal and abnormal states of the tool. The reliability of the comprehensive model was as high as 91.2% [11]. Ma et al. put forward a methodology for monitoring tool wear, which employed vibration singularity analysis and stacked LSTM. This method employed the Holder index to analyze the singularity of the original vibration signal, thereby eliminating the poor influence, and extracted and reduced sensitive features using the Pearson correlation coefficient. The method's accuracy was superior to various comparative models [12].

Despite the notable advancements achieved by existing approaches in the realm of tool wear identification and monitoring, several critical limitations persist. Firstly, when processing high-dimensional features and large-scale data, these methods suffer from high computational complexity and substantial time consumption. Moreover, the parameter optimization process is excessively reliant on hardware resources. Secondly, the fusion of features from multi-source heterogeneous signals is prone to noise interference or inadequate synchronization. This leads to feature redundancy and a decline in real-time monitoring efficiency. Thirdly, the recognition accuracy for rare types of tool wear, such as sudden fatigue wear, remains inadequate. Additionally, the models exhibit poor stability when confronted with imbalanced data distributions. In light of the aforementioned challenges, this research proposes a recognition and classification model based on SVM-WOA, alongside a prediction model built on ConvLSTM-AM. The primary aim is to accomplish high-precision and low-latency monitoring and prediction of tool wear states. This is achieved by enhancing the efficiency of parameter optimization, strengthening the extraction of spatio-temporal features, and incorporating an AM.

2. DESIGN OF IDENTIFICATION AND MONITORING METHODS

To achieve accurate identification and monitoring of hard alloy end mills, WOA is first used to optimize SVM, thereby improving the accuracy of the classification model. Secondly, to ensure that the hard alloy end mill has a longer service life, a new prediction model for end mill wear is developed by combining ConvLSTM and AM.

2.1 Design of Wear State Recognition Model for Hard Alloy End Milling Cutter with SVM-WOA

Currently, SVM, as a supervised learning model, has been widely applied in various classification and regression problems. In the problem of identifying the wear state of hard alloy end mills, SVM can effectively extract wear features and achieve accurate classification, thereby accurately determining the wear stage of milling cutters. In addition, SVM can also achieve maximum classification of data points in the feature space by constructing hyperplanes, thereby establishing clear boundaries between different categories. Figure 1 shows the optimal hyperplane classification process of SVM.

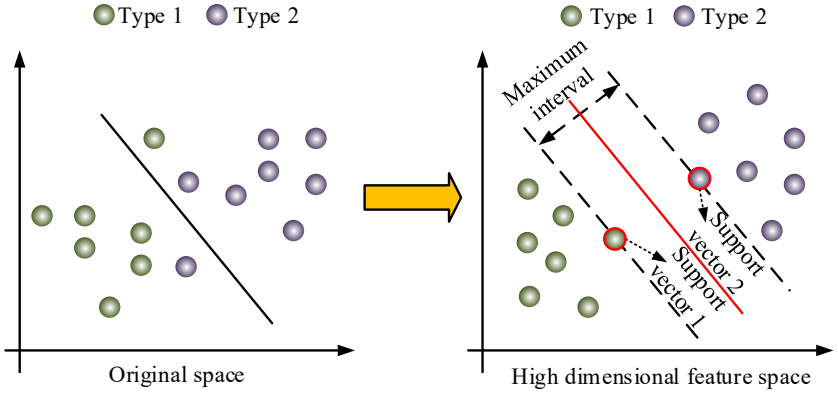

Figure 1. Schematic diagram of SVM optimal hyperplane

For nonlinear data, SVM uses the kernel function to map the data to a high-dimensional space, making it linearly separable and ensuring the global optimality of the solution. New samples are classified based on their distances from the hyperplane: positive distances are of the same class, and negative distances are of different classes. The maximization of intervals and classification errors is balanced through regularization parameters, thereby enhancing the generalization ability of the model. To address these issues, the study introduces WOA to optimize SVM. WOA has strong global search capability and fast convergence speed, which can more effectively find the optimal parameter combination, thereby improving the classification performance and recognition accuracy of SVM. The bubble predation process in the WOA is shown in Figure 2.

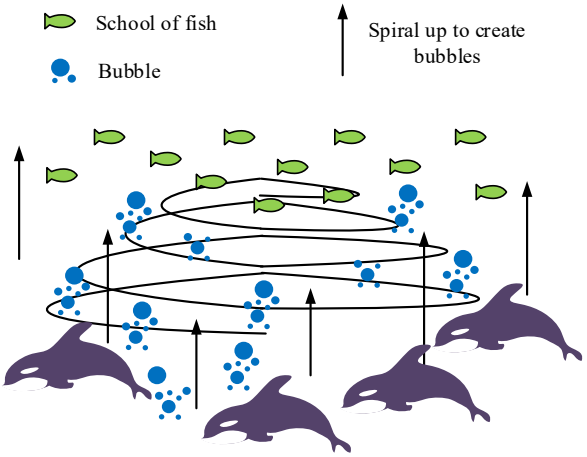

Figure 2. Schematic diagram of whale bubble feeding

Figure 2 shows the process of whales hunting through bubbles. In Figure 3, whales create a feeding trap by spiraling upwards to produce bubbles. Finally, the optimal solution for local search is achieved by narrowing the bubble range. The calculation equation for surrounding prey is shown in equation (1) [13-15].

$$\begin{cases} D = \left| C \cdot X^*(i) - X(i) \right| \\ X(i+1) = X(i) - AD \end{cases} \tag{1}$$

In equation (1), X^* represents the position of the prey; X indicates the positions of other whales; t indicates the number of iterations; i indicates the number; both A and C represent vector coefficients. D indicates the process of surrounding prey. By adjusting A and C, the optimal prey position can be found. The expression equation for A and C are shown in equation (2).

$$\begin{cases} A = 2\alpha r_1 - \alpha \\ C = 2r_2 \end{cases} \tag{2}$$

In equation (2), r_1 and r_2 respectively represent two vectors with different value ranges, ranging from 0 to 1. α represents the convergence factor. There are two ways of foaming attack. Equation (3) shows the calculation equation for the shrink wrap mechanism.

$$A' = 2\alpha \times rand_1 - \alpha \tag{3}$$

In equation (3), $rand_1$ denotes the random number between $[0,1]$, and A' represents the threshold parameter. Equation (4) is the calculation equation for the spiral update.

$$X(i+1) = De^{b'l} \cos(2\pi l) + X^*(i) \tag{4}$$

In equation (4), b' represents the constant of the spiral equation, usually taken as 1. represents the random number within the interval $[-1,1]$, where e represents the base of the natural number pair. D represents the distance between the current optimal solution and the current position of the individual. WOA is used to optimize SVM. Firstly, the kernel width of the radial basis function and the range of penalty factors in SVM are determined to ensure that WOA can search for the optimal combination within a reasonable range. Secondly, the search boundary of WOA is set, and the classification accuracy is used as the optimization objective, with the classification error rate as the fitness function of WOA. During this process, WOA generates multiple search particles, each representing a combination of a kernel parameter and a penalty factor. In addition, WOA will continuously adjust and update particle positions and search for the global optimal solution within the maximum iteration count by mimicking whale hunting behavior. Finally, through multiple iterations, WOA can find the optimal search particle position with the lowest classification error rate, and the corresponding kernel parameters and penalty factors for this position are the optimal combination of the SVM model. The classification and recognition model combining SVM and WOA will be designated as SVM-WOA, and the process of SVM-WOA completing the recognition and classification of the wear state of hard alloy end mills is shown in Figure 3.

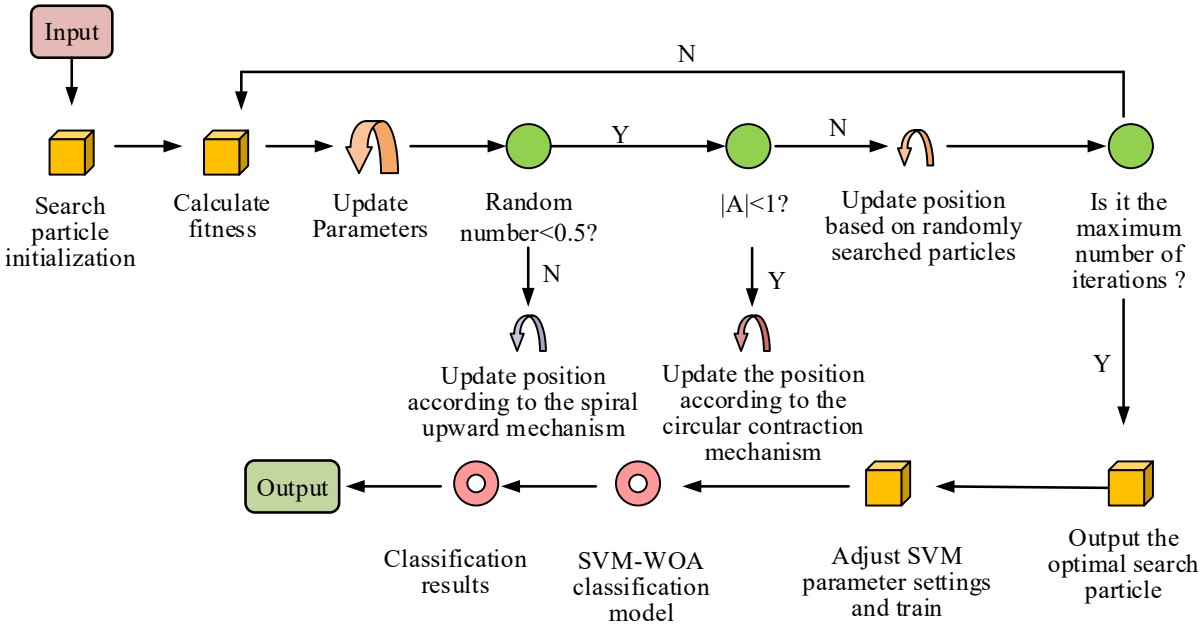

Figure 3. SVM-WOA flow chart

In Figure 3, the population is initialized to ensure that all particles are within the set value range. Subsequently, the fitness of each particle is calculated, with the classification error rate employed as the fitness function. The particle with the smallest fitness is found as the optimal particle. Subsequently, the particle position is updated according to the position update equation, and the optimal particle is updated when the fitness is better. Afterwards, it is determined whether the maximum iteration count has been reached. If not, the iteration continues until the optimization is completed.

2.2 Design of Wear Prediction Model for Hard Alloy End Mills Based on Improved ConvLSTM

In the practical application of hard alloy end mills, in addition to using the SVM-WOA model to identify and classify defective tools, it is also required to ensure that the tool's service life can be effectively extended and that the tool's usage can be monitored in real time. To address this challenge, ConvLSTM and AM from deep learning were introduced, and a ConvLSTM-AM model was built to predict the wear of end mills. The structure of the ConvLSTM-AM model is shown in Figure 4.

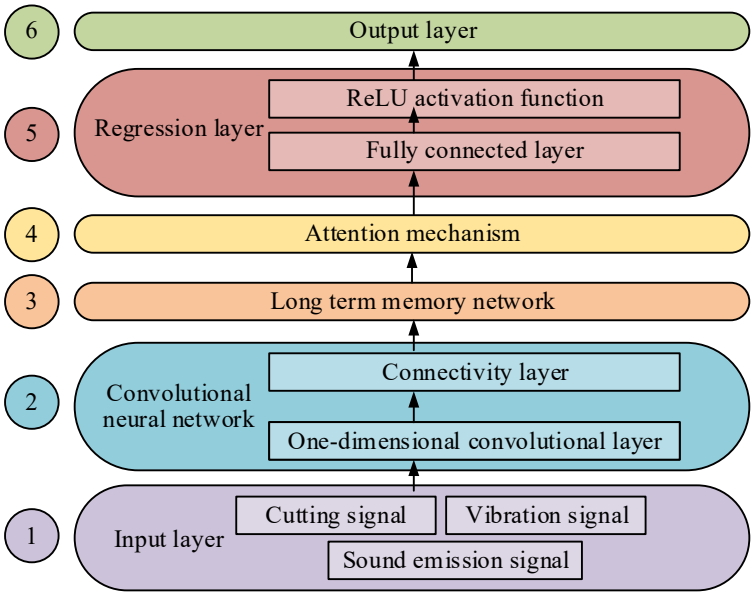

Figure 4. Structure diagram of ConvLSTM-AM

In Figure 4, the ConvLSTM-AM model for predicting the wear of hard alloy end mills is composed of multiple key components. Firstly, the input layer receives various cutting, vibration, and sound emission signals. The vibration signal is collected by the piezoelectric acceleration sensor, covering the mechanical vibration characteristics in the 0-10 kHz frequency band. The acoustic emission signal captures the high-frequency stress waves generated by the contact between the tool and the workpiece through a wideband acoustic emission sensor. The cutting force signal is synchronously recorded by the dynamic force sensor to quantify the time-domain fluctuations of the axial and radial component forces.

After the original signal undergoes anti-aliasing filtering, amplitude normalization and time sequence alignment, it is input into the model in the form of a multi-channel time series to ensure the integrity of spatial and temporal features.

The preprocessing process of the original signal consists of several major steps: (1) Anti-aliasing filtering: The Butterworth low-pass filter (cut-off frequency 10kHz, order 8) is used to eliminate high-frequency noise; (2) Amplitude normalization: The signals of each sensor are mapped to the [-1,1] interval through the Z-score standardization method to eliminate dimensional differences; (3) Timing alignment: Based on the dynamic time warping algorithm, the time of multi-source signals is synchronized to ensure the consistency of sampling intervals; (4) Data slicing: The continuous signal is segmented with a time window of 500ms (including 5,000 sampling points) to generate multi-channel time series inputs. The final data dimension is "sample size ×5000×3", including the characteristics of three channels: vibration, acoustic emission and cutting force.

Next, a One-Dimensional Convolutional Neural Network (1D-CNN) extracts spatial features through one-dimensional convolutional layers and multi-layer convolutional connection layers. These features are then passed to the LSTM. The model architecture is designed as follows: The 1D-CNN module consists of three layers of one-dimensional convolution, with the convolution kernel sizes being 64, 32, and 16, respectively. The number of channels multiplies layer by layer to 256. Each layer is followed by a ReLU activation function and a maximum pooling layer of size 2 for extracting local spatial features. The bidirectional LSTM module sets up 256 hidden-layer neurons, with the time step size consistent with the length of the input sequence (5000 steps) and introduces a Dropout rate of 0.3 to suppress overfitting. The AM adopts a four-head self-attention structure, with the key and query dimensions being 64. The time step weights are dynamically allocated through the Softmax function to enhance the expression ability of key features. The regression layer is composed of a fully connected layer of 128 neurons connected in series with the Sigmoid activation function, and finally outputs the normalized predicted wear amount value.

Based on the LSTM layer, AM is added to enhance the attention to important time step features by calculating attention weights, further improving the predictive ability of the model. Finally, the regression layer processes the features output by the LSTM layer through a fully connected layer and performs regression using an activation function, and then outputs the predicted wear amount. The structure of the 1D-CNN part in the ConvLSTM-AM model is shown in Figure 5 [16-18]. In Figure 5, the input layer is responsible for receiving tool wear data in a one-dimensional state. Finally, the fully connected layer integrates and maps the extracted features and outputs the final detection result. To improve the gradient vanishing problem in the feature extraction process of 1D-CNN, batch normalization, ReLU function, and max pooling layer are added after each convolutional layer for optimization [19-21]. After completing the data feature extraction task using ID-CNN, the output results will be entered into LSTM, and LSTM will be used to mine the temporal relationship between the end mill wear feature vectors. Figure 6 shows the structure of an LSTM.

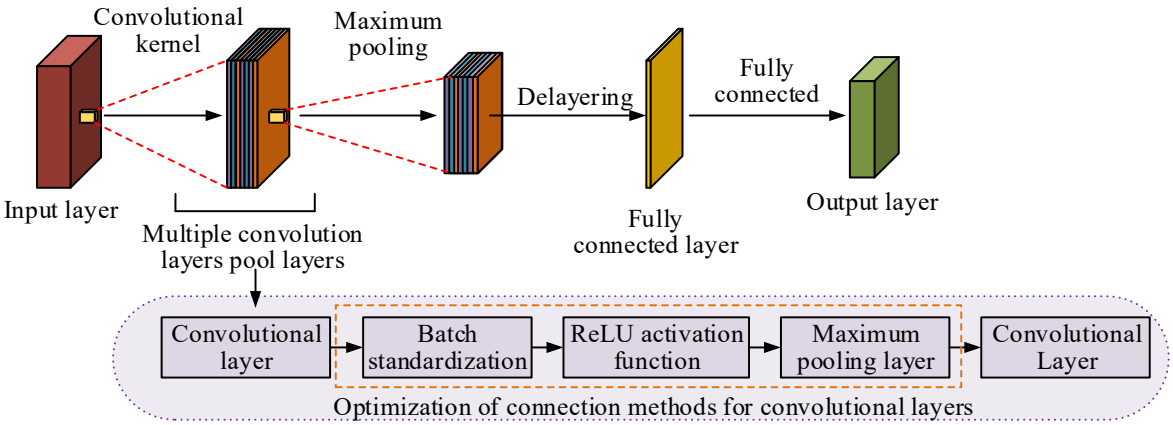

Figure 5. ID-CNN structure diagram

The LSTM model structure in Figure 6 consists of three key components: the input gate determines which new information needs to be updated or added to the memory unit, ensuring that the model captures key information related to the current state at each time step. The input gate processes a linear combination of the current input data. The forget gate assumes the function of filtering and deleting unnecessary information. This gating mechanism filters existing information in memory units to determine which information should be retained and which information needs to be forgotten or discarded [22-23]. This process is achieved by weighting the current input data and controlling the opening and closing degree of the forget gate through an activation function. After processing through the input gate and forget gate, the updated memory unit state will be output through the output gate. The main role of an output gate is to exert control over the hidden state of the current time step and then present it as an output, which will be utilized as the input for the next time step.

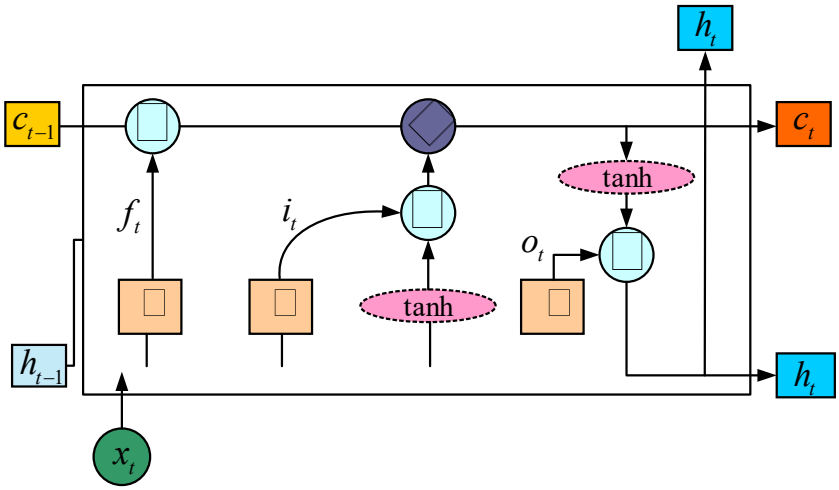

Figure 6. Structure diagram of LSTM neurons

By selectively filtering and processing the states of memory units, the output gate can ensure that the model conveys effective state information during the processing of time series data, while avoiding interference from irrelevant information. In LSTM, the calculation equation for the forget gate is as follows [24-26].

$$f_t = \sigma\left(W_f \cdot \left[h_{t-1}, x_t\right]\right) + b_f \tag{5}$$

In equation (5), f_t, b_f, and W_f respectively represent the forget gate, its bias vector, and the weight matrix. h_{t-1} and x_t respectively represent the hidden layer at time $t-1$ and the input of the previous cell at time t. σ represents the activation function sigmoid. The calculation equation for the input gate is further obtained as shown in equation (6).

$$i_t = \sigma\left(W_i \cdot \left[h_{t-1}, x_t\right] + b_i\right) \tag{6}$$

In equation (6), i_t, W_i, b_i respectively represent the input gate, its weight matrix, and bias vector. The calculation equation for the output gate is shown in equation (7).

$$o_t = \sigma\left(W_o \cdot \left[h_{t-1}, x_t\right] + b_o\right) \tag{7}$$

In equation (7), o_t, W_o, and b_o respectively denote the output gate, its weight matrix, and bias vector. Equation (8) shows the calculation equation for the cell state.

$$c_t = f_t \otimes c_{t-1} + i_t \otimes s_t \tag{8}$$

In equation (8), c_t and c_{t-1} denote the cell states at time t and $t-1$, respectively. s_t denotes the output value of the memory unit, and its detailed calculation equation is shown in equation (9).

$$s_t = \tanh\left(W_c \cdot \left[h_{t-1}, x_t\right] + b_c\right) \tag{9}$$

In equation (9), W_c and b_c denote the input gate weight matrix and bias vector, respectively. The calculation equation for the final output of the model is shown in equation (10).

$$h_t = o_t \cdot \tanh\left(c_t\right) \tag{10}$$

In equation (10), h_t represents the final output. After the features of the worn data are processed by the LSTM layer, they will enter the AM layer for further enhancement. The AM is a simulation mechanism that improves the accuracy of the deep learning network output by giving higher weights to key parts. The calculation equation for the attention weight values is shown in equation (11).

$$a_i = soft\max\left(s\left(h_t, q\right)\right) = \frac{\exp\left(s\left(h_t, q\right)\right)}{\sum_{i=1}^{t} s\left(h_t, q\right)} \tag{11}$$

In equation (11), $s(\cdot)$ represents the attention rating function, q represents the query vector, and a_i represents the attention weight. After passing through the AM layer, the data features will enter the regression layer, where the final predicted value is calculated through the nonlinear regression. The Mean Squared Error (MSE) loss function is selected as the loss function for the ConvLSTM-AM model, and its calculation equation is shown in equation (12).

$$Loss(Y,y)=\frac{1}{t'}\sum_{i=1}^{t'}(Y_i,y_i)^2 \tag{12}$$

In equation (12), y represents the actual wear value, Y represents the monitoring value, t' represents the number of samples, and $t'\in[1,2,\cdots,i]$. The model training adopted the Adam optimizer. The initial learning rate was set at 0.001, the momentum decay factors β1 and β2 were taken as 0.9 and 0.999, respectively, the batch size was 64, and the max iteration count was 200. To improve the generalization ability, an early stop mechanism was introduced during the training process. If the loss of the validation set did not decrease for 20 consecutive rounds, the training was terminated, and L2 regularization (coefficient 1×10^{-4}) was applied to constrain the weight parameters. The loss function selected the MSE. Meanwhile, the MAE and R^2 scores were used as auxiliary evaluation indicators to comprehensively quantify the prediction performance of the model.

3. RESULTS AND DISCUSSION

Firstly, the recognition and classification performance of the SVM-WOA model for end mill wear data was tested. Through indicators such as fitness value, iteration curve and confusion matrix, it was demonstrated that the SVM-WOA model had good classification performance. Secondly, the predictive performance of the ConvLSTM-AM model for end mill wear at different stages was tested. Through indicators such as wear error, average wear prediction accuracy, and average wear prediction time, it was demonstrated that ConvLSTM-AM could effectively predict the wear of end mills at different stages.

3.1 Classification Results of End Mill Wear Recognition Based on SVM-WOA

The study selected the publicly available NASA milling dataset as the experimental dataset, which contained the wear data of end mills under different cutting conditions. The dataset contained files in two common formats (i.e., .csv and .mat), which were used to record and analyze the milling process under different experimental operating conditions, with a particular focus on the evaluation and analysis of tool wear. The dataset was collected through three key sensing technologies. The acoustic emission sensor monitored the signals generated by the release of internal stress in the material during the milling process. The vibration sensor recorded the vibration mode of the machine tool and its components during the milling operation. The current sensor is an indirect indicator reflecting the motor load and the working status of the cutting tool. The sampling rate of NASA's milling dataset ranged from 10 kHz to 50 kHz. When conducting the test, 70% was divided into the training set and 30% into the test set. SVM, Particle Swarm Optimization Support Vector Machine (PSO-SVM), and Genetic Algorithm Neural Network (GANN) were selected as comparison models, and the fitness value iteration of the four models in the training set is shown in Figure 7.

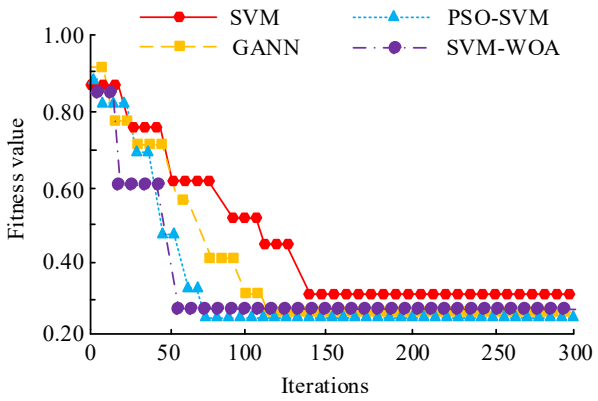

Figure 7. Iteration curves of fitness values of different classification models

Figure 7 shows the fitness iteration curves of four classification models: SVM, GANN, PSO-SVM, and SVM-WOA. In Figure 7, SVM, GANN, PSO-SVM, and SVM-WOA could reach a stable state after 131, 117, 69, and 53 iterations, respectively. At this point, the optimal fitness values for the four models were 0.31, 0.26, 0.25, and 0.28, respectively. Four common types of wear, namely cutting wear (referred to as Type 1), scraping wear (referred to as Type 2), fatigue wear (referred to as Type 3), and adhesive wear (referred to as Type 4), were selected as the classification and recognition criteria for the confusion matrix. After multiple recognition tests, the classification accuracy of the four models for different wear categories was shown in Figure 8.

Figure 8 shows the confusion matrix results of SVM, GANN, PSO-SVM, and SVM-WOA, respectively. In Figure 8, the optimal accuracies of SVM, GANN, PSO-SVM, and SVM-WOA in multiple classification tests were 0.856, 0.881, 0.916, and 0.989, respectively. This indicated that SVM-WOA had the best classification performance in multiple tests. Table 1 shows the average classification accuracy and average classification time of the four models for the four types of wear, which were further tested.

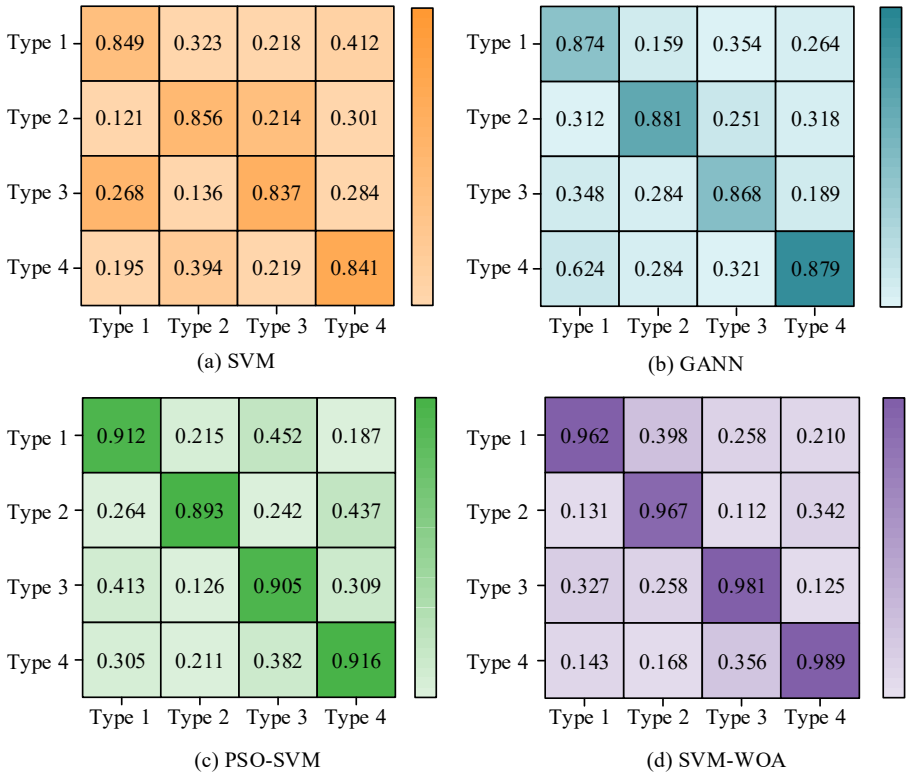

Figure 8. Confusion matrix results of different models

Table 1. The effect of different classification models to identify four kinds of wear tools

Algorithm	Wear type	Average classification accuracy (%)	Average sorting time (s)
SVM	Type 1	83.59%	12.06s
	Type 2	82.34%	11.95s
	Type 3	83.08%	11.82s
	Type 4	82.16%	12.15s
GANN	Type 1	87.76%	7.21s
	Type 2	88.24%	7.58s
	Type 3	87.15%	6.96s
	Type 4	88.20%	7.63s
PSO-SVM	Type 1	92.56%	5.34s
	Type 2	92.98%	5.28s
	Type 3	93.14%	4.97s
	Type 4	92.37%	5.19s
SVM-WOA	Type 1	98.21%	1.21s
	Type 2	99.05%	1.15s
	Type 3	98.45%	1.36s
	Type 4	97.82%	1.28s

In Table 1, the SVM-WOA model had an average classification accuracy of over 97% for all four types of wear, with Type 2 having the highest average classification accuracy of 99.05%. On the contrary, SVM had the highest average classification accuracy (83.59%) and the lowest of 82.16% for the four types of wear. In terms of average classification time, SVM, GANN, PSO-SVM, and SVM-WOA all had an average classification time of less than 15 seconds, but SVM-WOA had the best average classification time performance, with the lowest average classification time of only 1.15 seconds.

3.2 Prediction Results of End Mill Wear Based on ConvLSTM-AM

After demonstrating the effectiveness of the SVM-WOA model in tool wear recognition and classification tasks, the study further selected LSTM, Mask Region-based Convolutional Neural Network (Mask RCNN), and AM-based LSTM (Att LSTM) as comparative models to test the predictive performance of LSTM, Mask RCNN, Att LSTM, and ConvLSTM-AM in different stages of tool wear, as shown in Table 2.

Table 2. Different models predict the effect of three tool wear stages

Model	Wear stage	Average prediction accuracy (%)	Average forecast time (s)
LSTM	Stage 1	81.35	16.62
	Stage 2	81.83	18.25
	Stage 3	82.91	18.47
Mask-RCNN	Stage 1	85.66	11.05
	Stage 2	86.72	13.24
	Stage 3	86.94	12.69
Att-LSTM	Stage 1	91.20	8.74
	Stage 2	90.87	9.13
	Stage 3	91.56	8.58
ConvLSTM-AM	Stage 1	97.79	3.23
	Stage 2	97.25	3.86
	Stage 3	98.64	3.01

In Table 2, Stage 1, Stage 2, and Stage 3 represent the initial wear stage, intermediate wear stage, and severe wear stage experienced by the end mill during the wear process, respectively. Compared with the other three comparison models, ConvLSTM-AM performed well in predicting the wear stage of end mills, with an average prediction accuracy of up to 98.64%, far higher than LSTM's 82.91%, and an average prediction time as low as 3.01s, far lower than LSTM's 16.62s. The error performance of four models in the prediction process was compared, and the MSE and MAE curves shown in Figure 9 were obtained.

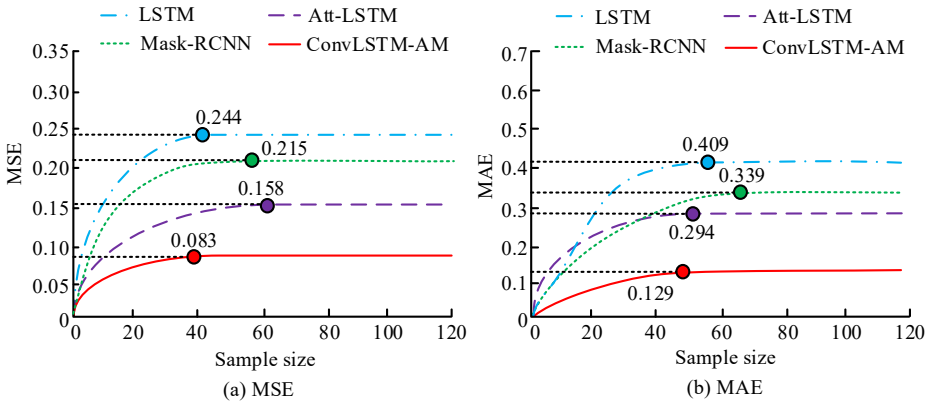

Figure 9. Error performance of different prediction models

Figures 9 (a) and 9 (b) show the MSE and MAE curves of LSTM, Mask RCNN, Att LSTM, and ConvLSTM-AM in prediction tasks, respectively. In Figure 9 (a), as the number of predicted samples increased, the MSE values of LSTM, Mask RCNN, Att LSTM, and ConvLSTM-AM also showed a trend of first increasing and then stabilizing, ultimately remaining at 0.244, 0.215, 0.158, and 0.083, respectively. In Figure 9 (b), as the MAE values stabilized, the maximum MAE values for LSTM, Mask RCNN, Att LSTM, and ConvLSTM-AM were 0.409, 0.339, 0.294, and 0.129, respectively. Figure 10 shows the predictive performance of four models for the three stages of wear, which were compared.

Figure 10 shows the prediction results of LSTM, Mask RCNN, Att LSTM, and ConvLSTM-AM models for end mill wear data at different wear stages, respectively. In Figure 10, compared to the other three models, ConvLSTM-AM could more accurately predict the wear amount at different stages, and its predicted values were basically consistent with the true values. To further verify the performance and reliability of the research method, a new open milling dataset collected from the industrial field was selected for research and analysis. This dataset, through synchronous collection by multiple sensors in the actual processing environment (vibration, acoustic emission, cutting force), recorded a total of 968 milling cycles of 14 types of cutting tools from the start of use to damage (each cycle contains 20,000 sampling points). In terms of data augmentation, overlapping samples were generated by sliding through a time window (with a step size of 250ms), expanding the original data volume to three times the original size, in order to alleviate the problem of data imbalance and improve the generalization ability of the model. During the experiment, the training set and the test set were divided in a ratio of 7:3. The prediction performances of different methods are shown in Table 3 as follows.

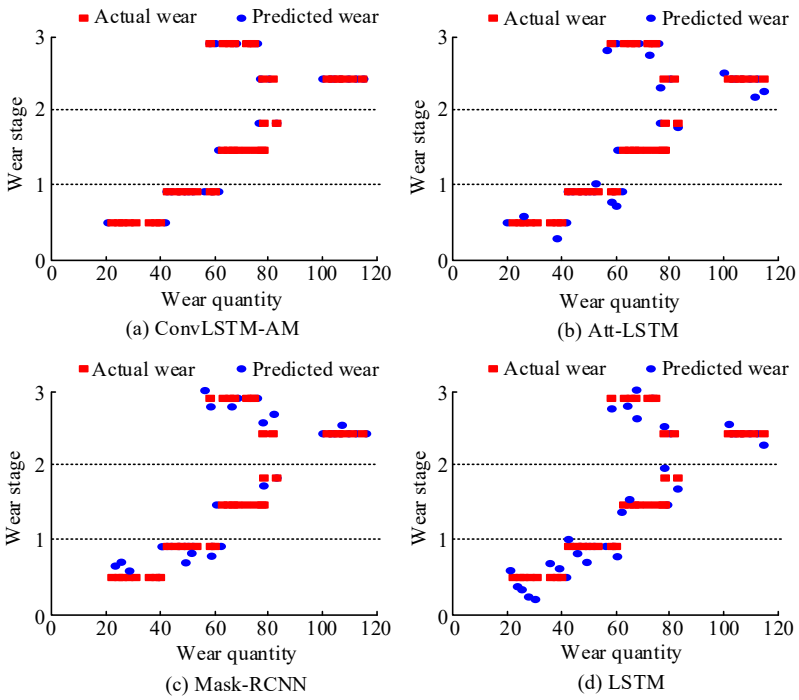

Figure 10. Actual prediction results of four models for three wear stages

Table 3. Prediction performance of different methods

Model	Wear Stage	Average Prediction Accuracy (%)	Average Prediction Time
LSTM	Stage 1	81.35	16.62
	Stage 2	81.83	18.25
	Stage 3	82.91	18.47
Mask RCNN	Stage 1	85.66	11.05
	Stage 2	86.72	13.24
	Stage 3	86.94	12.69
Att LSTM	Stage 1	91.20	8.74
	Stage 2	90.87	9.13
	Stage 3	91.56	8.58
ConvLSTM-AM	Stage 1	97.79	3.23
	Stage 2	97.25	3.86
	Stage 3	98.64	3.01

From Table 3, ConvLSTM-AM stood out with the highest prediction accuracy, reaching 98.64% at Stage 3 and performed significantly faster than LSTM and Mask RCNN, with a prediction time of just 3.01 seconds. The model's prediction performance was considerably superior to the others, especially in terms of both accuracy and time. This indicated that the research method had stronger operational performance. The Receiver Operating Characteristic (ROC) curves of different methods were analyzed, as shown in Figure 11.

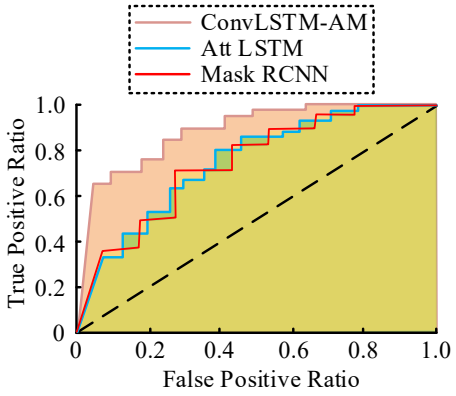

Figure 11. ROC curve

From Figure 11, the ROC curves of the three algorithms were all close to the upper left. The ROC Curve of the ConvLSTM-AM algorithm was above the Att LSTM algorithm and the Mask RCNN algorithm, and the Area Under the Curve (AUC) was 0.904. The ROC curves of the Att LSTM algorithm and the Mask RCNN algorithm partially intersect. The AUC value of the Att LSTM algorithm was 0.755, which was slightly higher than that of the Mask RCNN algorithm. This indicated that the error rate of the research method was lower compared with other algorithms.

4. CONCLUSIONS

To enhance the recognition and classification accuracy of the wear status of current hard alloy end mills, SVM-WOA and ConvLSTM-AM were employed to construct models for recognizing and classifying wear, and predicting wear, respectively. In the experiment to identify the wear state of hard alloy end mills, SVM-WOA performed well in classification tasks for different wear types, achieving significantly higher classification accuracy than SVM, PSO-SVM, and GANN. The accuracy rate of the research method remained above 97% in both datasets. In the classification test of four types of wear, the average classification accuracy of SVM-WOA reached the highest 99.05%, with an average time of only 1.15 seconds. In terms of wear prediction, ConvLSTM-AM achieved an average prediction accuracy of up to 98.64% across different wear stages, significantly outperforming other comparative models. In terms of average prediction time, ConvLSTM-SA had an average prediction time of only 3.01 seconds for stage 3, which was much lower than the 16.62 seconds for LSTM prediction stage 1. Additionally, ConvLSTM-SA achieved low MSE and MAE values in the prediction error test, which were 0.083 and 0.129, respectively.

The research method not only brought about substantial enhancements in computational efficiency and classification accuracy but also held significant industrial application value. By real-time monitoring and high-precision prediction of the tool wear state, this model could effectively reduce unplanned downtime caused by sudden tool failure, thereby ensuring the continuity and stability of the production line and significantly improving processing efficiency. Meanwhile, precise wear prediction enabled enterprises to formulate scientific maintenance strategies, avoiding resource waste caused by premature tool replacement or equipment damage resulting from delayed replacement, and significantly reducing production costs.

In future research, the lightweighting of models and the deployment of edge computing can be explored. Through technologies such as model compression and quantization, the demand for computing resources can be reduced, making them suitable for embedded devices or industrial edge nodes, thereby enhancing the real-time performance and flexibility of on-site applications. Furthermore, it is necessary to further verify the model's generalization ability for other tool types (such as drill bits and ball-end milling cutters) and enhance its universality through training on multi-material and multi-condition datasets. Additionally, the feasibility of integrating the model into the numerical control system can be investigated. For instance, a communication interface can be developed between the real-time monitoring module and the CNC controller to achieve closed-loop control of wear prediction and dynamic adjustment of processing parameters, thereby enhancing the autonomous decision-making ability of the intelligent manufacturing system. It is also possible to combine transfer learning and incremental learning techniques to develop adaptive models that can cope with the dynamic changes of different tool materials, processing parameters, and environments, thereby reducing the cost of repetitive training.

CONFLICT OF INTEREST

The author declares that there are no conflicts of interest.

AUTHOR'S CONTRIBUTION

Pan Yang conducted experiments, recorded data, analyzed the results, and wrote a manuscript.

ACKNOWLEDGEMENTS

The research is supported by: Chongqing Municipal Education Commission, Analysis and Prediction of Wear States of Carbide End Mills in Milling 6061 Aluminum Alloy (KJQN202403601).

REFERENCES

[1] G. Zheng, W. Chen, Q. Qian, A. Kumar, W. Sun, and Y. Zhou, "TCM in milling processes based on attention mechanism-combined long short-term memory using a sound sensor under different working conditions," *International Journal of Hydromechatronics,* vol. 5, no. 3, pp. 243-259, 2022.

[2] Y. Cheng, X. Zhang, G. Zhang, W. Jiang, and B. Li. "Thermal error analysis and modeling for high-speed motorized spindles based on LSTM-CNN," *International Journal of Advanced Manufacturing Technology*, vol. 121, no. 5, pp. 3243-3257, 2022.

[3] C. Yang, J. Zhou, E. Li, H. Zhang, M. Wang, and Z. Li. "Milling cutter wear prediction method under variable working conditions based on LRCN," *International Journal of Advanced Manufacturing Technology*, vol. 121, no. 3, pp. 2647-2661, 2022.

[4] J. Purohit and R. Dave. "Leveraging deep learning techniques to obtain efficacious segmentation results," *Archives of Advanced Engineering Science*, vol. 1, no. 1, pp. 11-26, 2023.

[5] A. Darwish. "A data-driven deep learning approach for remaining useful life in the ion mill etching process," *Sustainable Machine Intelligence Journal*, vol. 8, no. 2, pp. 14-34, 2024.

[6] W. Huang, Y. Li, X. Wu, and J. Shen. "The wear detection of mill-grinding tool based on acoustic emission sensor," *The International Journal of Advanced Manufacturing Technology*, vol. 124, no. 11, pp. 4121-4130, 2022.

[7] A. S. Pyatykh, A. V. Savilov, and S. A. Timofeev. "Method of tool wear control during stainless steel end milling," *Journal of Friction and Wear*, vol. 42, no. 4, pp. 263-267, 2021.

[8] Y. Peng, Q. Song, R. Wang, and Z. Liu. "Intelligent recognition of tool wear in milling based on a single sensor signal The *International Journal of Advanced Manufacturing Technology*, vol. 124, no. 3, pp. 1077-1093, 2022.

[9] S. Wang, S. Yan, and Y. Sun. "Milling tool condition monitoring for difficult-to-cut materials based on NCAE and IGWO-SVM," *International Journal of Advanced Manufacturing Technology*, vol. 129, no. 3, pp. 1355-1374, 2023.

[10] M. Shah, V. Vakharia, R. Chaudhari, J. Vora, D. Y. Pimenov, and K. Giasin. "Tool wear prediction in face milling of stainless steel using singular generative adversarial network and LSTM deep learning models," *International Journal of Advanced Manufacturing Technology*, vol. 121, no. 1, pp. 723-736, 2022.

[11] J. S. Nam and W. T. Kwon. "A study on tool breakage detection during milling process using LSTM-autoencoder and Gaussian mixture model," *International Journal of Precision Engineering and Manufacturing*, vol. 23, no. 6, pp. 667-675, 2022.

[12] K. Ma, G. Wang, K. Yang, M. Hu, and J. Li. "Tool wear monitoring for cavity milling based on vibration singularity analysis and stacked LSTM," *International Journal of Advanced Manufacturing Technology*, vol. 120, no. 5, pp. 4023-4039, 2022.

[13] S. Sivaraman, N. Radhika and M. Abubaker Khan, "Machine Learning-Driven Prediction of Wear Rate and Phase Formation in High Entropy Alloy Coatings for Enhanced Durability and Performance," *IEEE Acces*, vol. 13, pp. 33956-33975, 2025.

[14] H. G. Demir and I. Yesilyurt. "A comparison of four machine learning techniques and continuous wavelet transform approach for detection and classification of tool breakage during milling process," *Transactions of the Canadian Society for Mechanical Engineering*, vol. 47, no. 1, pp. 26-42, 2022.

[15] S. Chauhan, R. Trehan, R. P. Singh and V. S. Sharma, "Assessment of machining performance for intelligent tool wear prediction using hybrid extreme learning machine," *IEEE Sensors Journal*, vol. 24, no. 22, pp. 37915-37922, 2024.

[16] N. Chu, W. Kang, X. Yao, and J. Fu, "Online roundness prediction of grinding workpiece based on vibration signals and support vector machine," *International Journal of Advanced Manufacturing Technology*, vol. 126, no. 5, pp. 2733-2743, 2023.

[17] D. Wang, C. Han, L. Wang, X. Li, E. Cai, and P. Zhang, "Surface roughness prediction of large shaft grinding via attentional CNN-LSTM fusing multiple process signals," *International Journal of Advanced Manufacturing Technology*, vol. 126, no. 11, pp. 4925-4936, 2023.

[18] J. Sharmila Devi and P. Balasubramanian, "Comparative analysis on recent deep learning techniques for identifying chatter in milling process," *Journal of Intelligent & Fuzzy Systems,* vol. 44, no. 3, pp. 3647-3666, 2023.

[19] Y. Quan, C. Liu, Z. Yuan and B. Yan, "Hybrid data augmentation combining screening-based MCGAN and manual transformation for few-shot tool wear state recognition," *IEEE Sensors Journal*, vol. 24, no. 8, pp. 12186-12196, 2024.

[20] Y. Liu, S. Yang, T. Sun, and Y. Zhang, "Milling tool wear prediction: optimized long short-term memory model based on attention mechanism," *Ferroelectrics*, vol. 607, no. 1, pp. 56-72, 2023.

[21] Y. Meng, Z. Dong, K. -C. Lu, S. Li and C. Shao, "Meta-learning-based domain generalization for cost-effective tool condition monitoring in ultrasonic metal welding," *IEEE Transactions on Industrial Informatics*, vol. 21, no. 1, pp. 653-662, 2025.

[22] Q. Hu, B. Su, J. Kong and W. Liu, "Adaptive wavelet convolution stochastic analysis graph neural network for remaining useful life prediction," *IEEE Sensors Journal*, vol. 25, no. 11, pp. 19428-19441, 2025.

[23] H. Sümbül, "A Novel Mems and Flex Sensor-Based Hand Gesture Recognition and Regenerating System Using Deep Learning Model," *IEEE Acces*, vol. 12, pp. 133685-133693, 2024.

[24] K. Ouyang, P. Hu, J. Liao and L. Yang, "Measurement method of 3-D rotation angle of spherical joint based on neural network and magnetic effect," *IEEE Sensors Journal*, vol. 24, no. 16, pp. 26866-26876, 2024.

[25] C. Ren, B. Jiang and N. Lu, "Federated learning with potential partnership identification for accurate prediction in flexible manufacturing system," *IEEE Transactions on Reliability*, vol. 74, no. 2, pp. 2549-2560, 2025.

[26] D. -M. Shi, T. Huang, X. -M. Zhang and H. Ding, "Superresolution restoration of cutting forces in thin-walled milling with a diffusion model," *IEEE/ASME Transactions on Mechatronics*, vol. 30, no. 2, pp. 1447-1458, 2025.